Molecular Therapy
Nucleic Acids
Original Article

Aptamer-programmable adeno-associated viral vectors as a novel platform for cell-specific gene transfer

Francesco Puzzo,[1] Chuanling Zhang,[1,2] Bethany Powell Gray,[3] Feijie Zhang,[1] Bruce A. Sullenger,[3] and Mark A. Kay[1]

[1]Departments of Pediatrics and Genetics, Stanford University, Stanford, CA 94305, USA; [2]State Key Laboratory of Natural and Biomimetic Drugs, School of Pharmaceutical Sciences, Peking University, Beijing 100191, China; [3]Department of Surgery, Duke University School of Medicine, Durham, NC 27705, USA

Adeno-associated viruses (AAVs) are commonly used for *in vivo* gene therapy. Nevertheless, the wide tropism that characterizes these vectors limits specific targeting to a particular cell type or tissue. Here, we developed new chemically modified AAV vectors (Nε-AAVs) displaying a single site substitution on the capsid surface for post-production vector engineering through biorthogonal copper-free click chemistry. We were able to identify AAV vectors that would tolerate the unnatural amino acid substitution on the capsid without disrupting their packaging efficiency. We functionalized the Nε-AAVs through conjugation with DNA (AS1411) or RNA (E3) aptamers or with a folic acid moiety (FA). E3-, AS1411-, and FA-AAVs showed on average a 3- to 9-fold increase in transduction compared with their non-conjugated counterparts in different cancer cell lines. Using specific competitors, we established ligand-specific transduction. *In vivo* studies confirmed the selective uptake of FA-AAV and AS1411-AAV without off-target transduction in peripheral organs. Overall, the high versatility of these novel Nε-AAVs might pave the way to tailoring gene therapy vectors toward specific types of cells both for *ex vivo* and *in vivo* applications.

INTRODUCTION

In the last two decades recombinant adeno-associated virus (AAV) vectors have been widely employed in many clinical trials, making these vectors the preferred delivery system for *in vivo* gene therapy.[1,2] Several groups, including ours, have developed novel AAV capsids through DNA shuffling or peptide display techniques to create vectors with improved transduction *in vivo*.[3] Thus, novel AAV vectors have been successfully engineered to enhance targeting to different organs including liver, brain, skeletal muscle, and eye, among others.[4] More recently, researchers have been using different approaches to synthetically modify AAV capsids to improve properties such as immune escape and receptor-specific cell targeting.[5,6]

In recent years, progress in synthetic biology has led to expansion of the genetic code by taking advantage of "unnatural" amino acids from prokaryotic microorganisms.[7] Consequently, researchers have been able to utilize them in mammalian systems and create hybrid proteins bearing unnatural amino acids in their structure. This was achieved by engineering pairs of orthogonal prokaryotic tRNA/tRNA synthases, which were genetically expressed in mammalian cells. Hence, the unnatural amino acid would be recognized by the mammalian translational machinery and inserted in the nascent polypeptide.[8] These unnatural amino acids have been mostly employed for studying protein functions or creating *de novo* protein properties for therapeutic purposes.[9] Recently, the use of the unnatural amino acids was applied to AAV engineering. In particular, the placement of an azido group (N_3) on the capsid surface allows click chemistry conjugation of molecules on AAV2.[10] Other chemical modifications of AAV vectors have been also described.[11,12] Nevertheless, these approaches are strictly dependent on the amino acid composition of the capsid surface, whereas particular insertion of a single unnatural amino acid onto a specific region of the capsid would allow specific conjugation of molecules onto the AAV regardless of capsid composition.

It has been described that the expression of folic acid receptor (hFOLR1) is highly upregulated in some types of cancers such as breast, ovarian, lung, and kidney malignancies, making hFOLR1 an intriguing targetable candidate for anti-tumor therapies.[13] Consequently, approaches where folic acid was conjugated to small interfering RNAs[14] or lipid nanoparticles[15] have been harnessed to target overexpressing-hFOLR1 cancer cells. Recently, researchers have also engineered chimeric antigen receptor T cells to target hFOLR1for the treatment of pediatric acute myeloid leukemia (AML).[16]

Moreover, nucleic acid-based molecules such as DNA and RNA aptamers have been utilized to specifically target tumor cells.[17] The high versatility of aptamers and their remarkable affinity for specific ligands allowed for rapid development and use in clinical trials.[18] In particular, the AS1411 DNA aptamer has been extensively characterized in the cancer research field,[19,20] and a phase I/II clinical trial was also completed to assess its safety and efficacy in patients.[21] Furthermore, a recently described E3 RNA aptamer has also been

Received 12 August 2022; accepted 19 January 2023;
https://doi.org/10.1016/j.omtn.2023.01.007.

Correspondence: Mark A. Kay, MD, PhD, Departments of Pediatrics and Genetics, Stanford University, 269 Campus Drive, Rm 2105, Stanford, CA 94305, USA.
E-mail: markay@stanford.edu

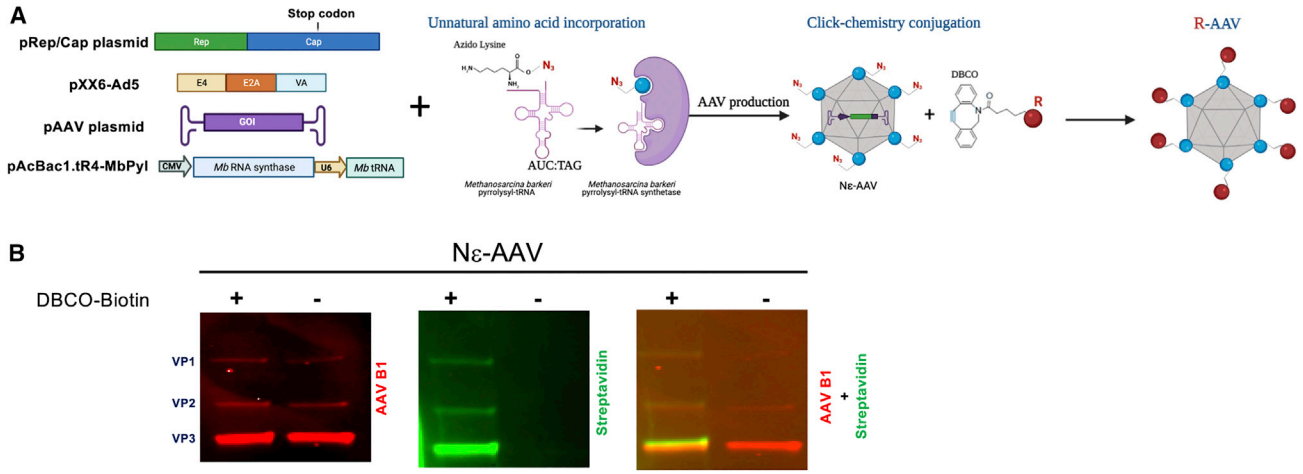

Figure 1. Nε-AAV vector production and conjugation

(A) Schematic representation of Nε-AAV production. Once the unnatural amino acid is incorporated into the AAV capsid, the exposed azido group (N_3) reacts with the DBCO resulting in the conjugation of R, where the "R" is a generic molecule (e.g., peptide, nucleic acid). (B) Western blot analysis of Nε-AAV upon conjugation with the DBCO-biotin molecule. An anti-AAV antibody, clone B1, was used to detect the VP1/2/3 capsid proteins of AAV. An anti-streptavidin antibody was used to detect the biotin-conjugated Nε-AAV vector.

characterized to specifically target and internalize into multiple cancer cells.[22,23]

Combining synthetic, molecular, and chemical biology, we have created a novel class of programmable AAV vectors, Nε-AAVs, by utilizing single unnatural amino acid insertion. We characterized different mutant capsids of Nε-AAV vectors and successfully conjugated them by click chemistry. Eventually, we successfully programmed the Nε-AAVs through conjugation to folic acid or DNA or RNA aptamers to target specific cancer cells. *In vivo* studies in xenograft animal models confirmed that the folic acid-conjugated AAV vectors and the DNA aptamer AS1411 conjugated AAV vectors led to highly specific uptake in the intended target cells.

RESULTS

Production of chemically modified AAV and click chemistry conjugation

We started by chemically modifying the AAV-DJ capsid, which was previously isolated in our lab, because of its efficiency in transducing many cells *in vitro* as well as its high titer production.[24]

Similar to what has been reported for AAV2 and AAV-DJ/8,[24,25] we ablated the heparan sulfate proteoglycan (HSPG) binding sites by substituting two alanines for two arginines at the 587 and 590 positions (hereafter referred as AAV-DJR/A) to reduce the infectivity of AAV-DJ *in vitro* (Figure S1A). Next, we employed a rational design based on the crystal structure of AAV-DJ[26] (https://www.rcsb.org) to introduce an amber stop codon (TAG) in different regions of the AAV-DJR/A capsid sequence (DJR/A-N589, DJR/A-D555, DJR/A-A587, and DJR/A-T456) as sites to replace the endogenous amino acid with the unnatural amino acid.

Consequently, the newly made capsids were used for AAV production using a CAG promoter-firefly luciferase expression cassette for *in vitro* experiments. The pAcBac1.tR4-MbPyl plasmid, which expresses a pyrrolysyl-tRNA and a pyrrolysyl-tRNA synthase, both derived from the *Methanosarcina barkeri*,[27] was added to the classical triple transfection protocol for AAV production. Finally, the unnatural amino acid, azido-lysine, was supplemented into the cell media during vector preparation (Figure 1A).

In the end, this creates an AAV-producing system in which the expression of the prokaryotic tRNA/tRNA synthase forces the mammalian translational system to recognize the UAG stop codon as a regular codon and incorporate the azido-lysine on the AAV capsid during the production of the chemically modified vector.[10] This novel AAV, which we call Nε-AAV, carrying a single azido-amino acid insertion on a specific capsid position, allowed us to conjugate any molecule containing a dibenzocyclooctyne chemical group (DBCO) to the capsid by simply performing a click chemistry reaction (Figure 1A). However, before the vector conjugation, we assessed the transduction of the newly produced Nε-DJR/A mutants in HeLa cells. We found that the Nε-DJR/A-N589 and Nε-DJR/A-A587 vectors resulted in slightly higher luciferase activity compared with the Nε-DJR/A-D555 and Nε-DJR/A-T456 vectors (Figure S1B).

Next, using a copper-free cycloaddition reaction,[28] we conjugated the Nε-DJR/A-N589 vector with a DBCO-biotin to detect the biotin-AAV by western blot using a streptavidin-labeled antibody. As shown

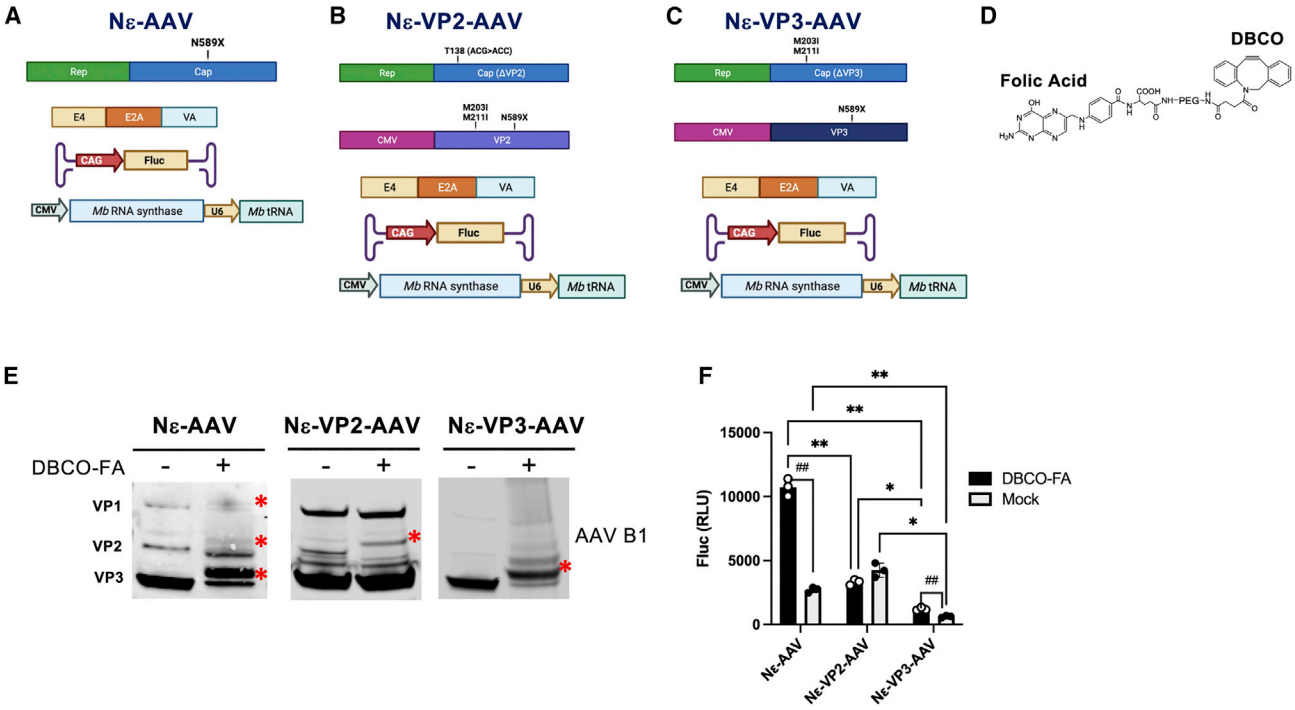

Figure 2. Development of the FA-AAV vector after folic acid conjugation

(A–C) Schematic representation of the plasmids used for (A) Nε-AAV, (B) Nε-VP2-AAV, and (C) Nε-VP3-AAV production. (D) Chemical formula of the DBCO-PEG (2K)-FA molecule used for the Nε-AAV vector conjugation. (E) Western blot analysis of Nε-AAV, Nε-VP2-AAV, Nε-VP3-AAV upon DBCO-PEG (2K)-FA conjugation. An anti-AAV antibody, clone B1, was used to detect the VP1/2/3 capsid proteins of AAV. Asterisks indicate the VP proteins where the folic acid has been conjugated. (F) Luciferase activity in HeLa cells after transduction with DBCO-FA-conjugated AAV vectors. Mock-conjugated Nε-AAV vectors were used as controls. Cells were transduced at 1,000 vector genomes (vg)/cell. Statistical analysis: for two-way ANOVA with Tukey's post hoc test, the statistical significance was assumed with p value of <0.05 (*), <0.01 (**), <0.001 (***), and <0.0001 (****); with Sidak's post hoc test the statistical significance was assumed with a p value of <0.05 (#), <0.01 (##), <0.001 (###), and <0.0001 (####). Error bars represent standard deviation.

in Figure 1B, both the unconjugated and conjugated Nε-AAV vectors were detected by the anti-AAV antibody AAVB1 (red signal), while the streptavidin antibody (green signal) recognized only the biotin-conjugated Nε-AAV. Notably, the streptavidin signal overlapped with the AAVB1 antibody (yellow signal), demonstrating the specific nature of the biotin conjugation on the AAV capsid proteins VP1/2/3 (Figure 1B).

These data confirm that the azido-lysine was successfully incorporated on the AAV capsid and that the DBCO-biotin was specifically conjugated to the Nε-AAV.

Design and characterization of Nε-AAVs upon folic acid conjugation

Since the Nε-AAV capsid incorporates the azido-lysine on each of the VP1, VP2, and VP3 proteins (Figure 2A), we also attempted to specifically target the insertion of the unnatural amino acid onto only the VP2 (Figure 2B) or VP3 (Figure 2C) proteins.

To insert the azido-lysine on VP2, we used a strategy described for other AAV vectors by making a single-nucleotide mutation at the DJR/A sequence to circumvent VP2 expression[29] (Nε-VP2-AAV, Figure 2B). Next, we created another rep/cap DJR/A plasmid to eliminate VP3 expression, and an additional plasmid that only expressed VP3[30] (Nε-VP3-AAV, Figure 2C).

Western blot analyses show that the Nε-VP2-AAV and Nε-VP3-AAV can be complemented with the plasmids expressing either VP2 (Figure S1C) or VP3 (Figure S1D). To functionalize the new chemically modified AAV vectors, we performed a click chemistry reaction using a DBCO-folic acid molecule with a 2 kDa polyethylene glycol (PEG) linker (DBCO-FA) (Figure 2D). As a negative control we used unconjugated Nε-AAV vectors. Western blot analysis showed that the DBCO-FA conjugation resulted in a shift in the specific VP capsid protein bands where the folic acid conjugation took place, as highlighted by the red asterisks in Figure 2E. This was further confirmed and shown in a silver-stained gel of folic acid-conjugated vector (Figure S1E). These data demonstrate that the unnatural amino acid insertion and consequent folic acid conjugation occurred either on all three VP1/2/3 proteins or specifically on VP2 and VP3 depending on the plasmid combination used for the vector production.

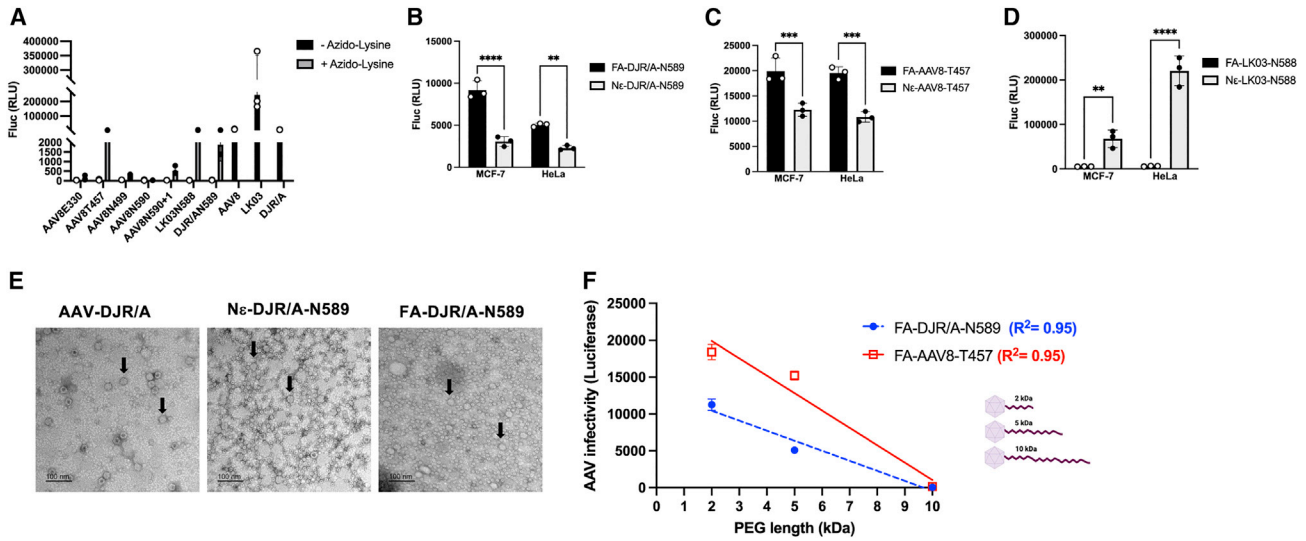

Figure 3. Assessment of novel Nε-AAV vectors upon folic acid conjugation

(A) Luciferase activity in HeLa cells of the Nε-AAV vectors produced in presence (+azido-lysine) or absence (−azido-lysine) of unnatural amino acid. AAV crude lysate was used for HeLa transduction evaluation. (B–D) Luciferase activity in HeLa and MCF-7 cell lines upon transduction with (B) FA-DJR/A-N589, (C) FA-AAV8-T457, and (D) FA-LK03-N588. The unconjugated Nε-AAV vectors were used as control. (E) Transmission electron microscopy images of AAV-DJR/A, unconjugated Nε-DJR/A-N589, and FA-DJR/A-N589 vectors. (F) Regression plot showing the reverse correlation between the length of the PEG linker and AAV vector infectivity of FA-AAV8-T457 and FA-DJR/A-N589 vectors. Statistical analysis (B–D): two-way ANOVA with Sidak's post hoc test; statistical significance was assumed with a p value of <0.05 (*), <0.01 (**), <0.001 (***), and <0.0001 (****). Error bars represent standard deviation.

Based on these results, we produced Nε-AAV vectors expressing luciferase and tested the folic acid-conjugated AAV vectors on cancer cell lines that are reported to express high levels of human folic acid receptor (hFOLR1)[31] (https://www.proteinatlas.org/ENSG00000110195-FOLR1; Figure S1F). In HeLa cells, the folic acid-conjugated Nε-AAV and Nε-VP3-AAV (DBCO-FA) showed significantly higher luciferase activity compared with the unconjugated Nε-AAV control vectors (mock) (Figure 2F). Notably, the FA-conjugated Nε-AAV displayed remarkably enhanced transduction efficiency compared with both the FA-conjugated Nε-VP2-AAV and Nε-VP3-AAV (Figure 2F). Moreover, the Nε-VP2-AAV and Nε-VP3-AAV vectors showed significantly decreased infectivity even when transduced at higher multiplicity of infection (MOI) (Figure S1G). Because the Nε-VP2-AAV and Nε-VP3-AAV displayed an overall reduced ability to transduce cells, we decided to use the Nε-AAV vectors in subsequent studies (Figure 2A).

Rational mutagenesis screen to identify novel Nε-AAV mutant capsids

After the successful conjugation of the AAV-DJR/A, we introduced the unnatural amino acid on the AAV8 and AAVLK03 capsids. Thus, using the same rational design as used for the Nε-AAV-DJR/A mutants, we generated new vectors with the azido-lysine displayed on the capsid surface.[26,32] We made eight new Nε-AAV variants (five AAV8 and three LK03 mutants, where the capital letter and the number next to the AAV serotype indicate the position and amino acid replaced by the azido-lysine on the vector capsid). Notably, all the new Nε-AAV vectors showed a lower titer compared with their wild-type counterparts (Figure S2A).

To test the infectivity of the new Nε-AAV mutants, we made luciferase-expressing vectors using either regular medium, where no vector is expected to be produced, or supplemented with azido-lysine, and assessed their infectivity on HeLa cells. For a quick assessment of transduction, we used crude AAV lysates. Among the new vectors only Nε-AAV8-T457 and Nε-LK03-N588 retained the ability to transduce cells when produced in the presence of azido-lysine, while Nε-DJR/A-N589 was used as control (Figure 3A). These three vectors were conjugated with the DBCO-PEG (2K)-FA and tested on three different cancer cell lines, HeLa, MCF-7, and A549. FA-DJR/A-N589 and FA-AAV8-T457 showed a significantly higher transduction efficiency compared with the unconjugated Nε-AAV controls (Figures 3B, 3C, S2B, and S2C). Conversely, FA-LK03-N588 failed to transduce HeLa, MCF-7, and A549 cells, possibly because the conjugation may have disrupted the vector infectivity (Figures 3D and S2D). Thus, it is possible that the AAV modification through unnatural amino acid incorporation depends on the capsid region where the unnatural amino acid is introduced, while other regions might not be permissive to this modification.

Introduction of the unnatural amino acid and folic acid conjugation did not show any structural differences based on transmission electron microscopy in the Nε-DJR/A-N589 and FA- DJR/A-N589 compared with the wild-type AAV-DJR/A vector (Figure 3E).

To evaluate whether the length of the PEG linker would affect the infectivity of the FA-AAV vectors, we conjugated the Nε-DJR/A-N589 and Nε-AAV8-T457 with DBCO-FA containing different lengths of PEG (2 kDa, 5 kDa, and 10 kDa). In MCF-7 cells, both the Nε-DJR/A-N589 and Nε-AAV8-T457 conjugated with the DBCO-FA-2k demonstrated a significant increase in luciferase activity compared with the vectors with longer PEG linkers, DBCO-FA-5k and DBCO-FA-10k, and the unconjugated Nε-AAV. Remarkably, the FA-AAVs also showed an increased infectivity compared with their wild-type counterparts DJR/A and AAV8, respectively (Figures S2E and S2F). Interestingly, we saw an inverse correlation between the length of the PEG linker and FA-AAV infectivity regardless of the Nε-AAV capsid utilized, whereby the increasing length of the linkers significantly reduced the AAV transduction (Figure 3F). These data demonstrate that an optimal distance between the AAV capsid and the conjugated molecule (folic acid in this case) is pivotal to maintaining the infectivity of the Nε-AAV vectors.

To rule out the possibility that the PEG, per se, might influence AAV infectivity, we conjugated the Nε-DJR/A-N589 with a DBCO-PEG moiety devoid of folic acid. Of note, the DBCO-PEG-conjugated AAV showed a significant reduction in transduction compared with both the unconjugated Nε-DJR/A-N589 and DJR/A AAV vectors (Figure S2G). Finally, we tested whether we could further improve the efficiency of DBCO-FA conjugation onto AAV by increasing its concentration during the click reaction step. To this end, incubating the Nε-DJR/A-N589 capsid with 2 mM versus 0.5 mM DBCO-FA increased the incorporation of FA into VP3 capsid protein (Figure S2H). Nevertheless, as already reported by Lee and colleagues,[33] the increase in the ratio between PEGylated molecules and AAV vector resulted in a loss of specific transduction efficiency, as we also observed for FA-DJR/A-N589 (Figure S2I).

FA-AAV-specific uptake *in vitro*

To further characterize the FA-AAV vectors, we set up an *in vitro* assay in which we co-cultured the cells with an excess of free folic acid, which should compete with the FA-AAVs for the hFOLR1 on the cell surface and eventually reduce the FA-AAV infectivity (Figure 4A). Indeed, the FA-DJR/A-N589 showed a dramatic 8-fold reduction in luciferase activity when HeLa cells were co-cultured with an excess of folic acid compared with cells without folic acid. Conversely, the unconjugated Nε-DJR/A-N589 and the DJR/A, used as controls, displayed a similar level of transduction regardless of whether the folic acid was added onto cells (Figure 4B). Furthermore, similar results were obtained with two different Nε-AAV vectors, FA-AAV8-T457 and FA-DJR/A-A587 (Figures 4C and 4D). Notably, when the same assay was performed on MCF-7 using the FA-DJR/A-N589 vector, the luciferase activity was massively reduced by ∼30-fold while the unconjugated Nε-DJR/A-N589 showed similar transduction levels with or without folic acid incubation (Figure 4E).

To further verify the specificity of the folic acid receptor-mediated uptake, we treated the cells with an antibody directed against the hFOLR1 (hFOLR1-Ab) to block its activity and, in turn, FA-AAV transduction (Figure 4F). As shown in Figure 4G, FA-DJR/A-N589 displayed a significant 2-fold decrease in luciferase levels when HeLa cells were pre-incubated with the hFOLR1-Ab compared with cells that were not treated with the antibody. In contrast, the unconjugated Nε-DJR/A-N589 and the DJR/A showed similar levels of transduction regardless of whether the cells were treated with hFOLR1-Ab. Similar results were obtained using FA-AAV8-T457, showing again that the FA-AAV transduction was folic acid dependent (Figure 4H). Of note, incubation with hFOLR1-Ab significantly decreased transduction by 3-fold in MCF-7 cells (Figure 4I).

Overall, the use of two independent assays and different Nε-AAVs corroborate that the uptake of the FA-AAV vectors was remarkably receptor- and FA-specific and independent of the AAV serotype.

In vitro characterization of aptamer-conjugated Nε-AAVs

In contrast to folic acid and peptide-derived molecules, we sought to conjugate the Nε-AAV vectors with nucleic acid ligands such as aptamers, since they have shown binding properties comparable with those of antibodies.[34] As proof of concept, we decided to evaluate one of the most characterized DNA aptamers utilized in cancer research, AS1411.[19] To conjugate the AS14411 aptamer to the Nε-AAV, we needed to first make a conjugable DBCO-AS1411 molecule. To this end, we combined a DBCO-PEG-NHS with an amine (NH_2) modified AS1411 aptamer to create DBCO-PEG-AS1411 (Figure 5A).

Subsequently, we conjugated the DBCO-PEG-AS1411 to the Nε-AAV vectors. To assess the AS1411-AAV conjugation, we designed a biotinylated oligonucleotide antidote that would specifically bind to the AS1411 aptamer. Thus, the AS1411-AAV would be detected by western blot using a streptavidin-conjugated antibody. Indeed, western blot analysis showed that only the AS1411-AAV can be detected by the streptavidin antibody (green signal) upon incubation with the biotinylated probe (Figure 5B). Notably, the overlapping signal (yellow) of streptavidin (green) and AAVB1 (red) antibodies show that the aptamer conjugation is specific to the VP2 capsid proteins on AS1411-AAV (Figure 5B). The reason for this apparent VP2-specific conjugation is still unknown. However, we cannot rule out the possibility that the conjugated aptamer is not fully recognized by the biotinylated oligo probe and that the denaturing conditions of the SDS-PAGE could mask or change aptamer availability on VP1 and VP3.

Moreover, as previously demonstrated with the FA-AAVs, we did not see any significant structural changes in the Nε-AAV capsid upon AS1411 aptamer conjugation (Figure S3A). Next, we conjugated the Nε-DJR/A-N589 vector expressing luciferase to the DBCO-PEG-AS1411 aptamer and transduced the MCF-7 breast cancer cell line.[35] We infected the cells with different amounts of AS1411-DJR/A-N589 and used the unconjugated Nε-DJR/A-N589 as a control. Notably, AS1411-DJR/A-N589 exhibited a remarkably enhanced infectivity compared with the unconjugated Nε-DJR/A-N589 at all tested MOIs (Figure 5C).

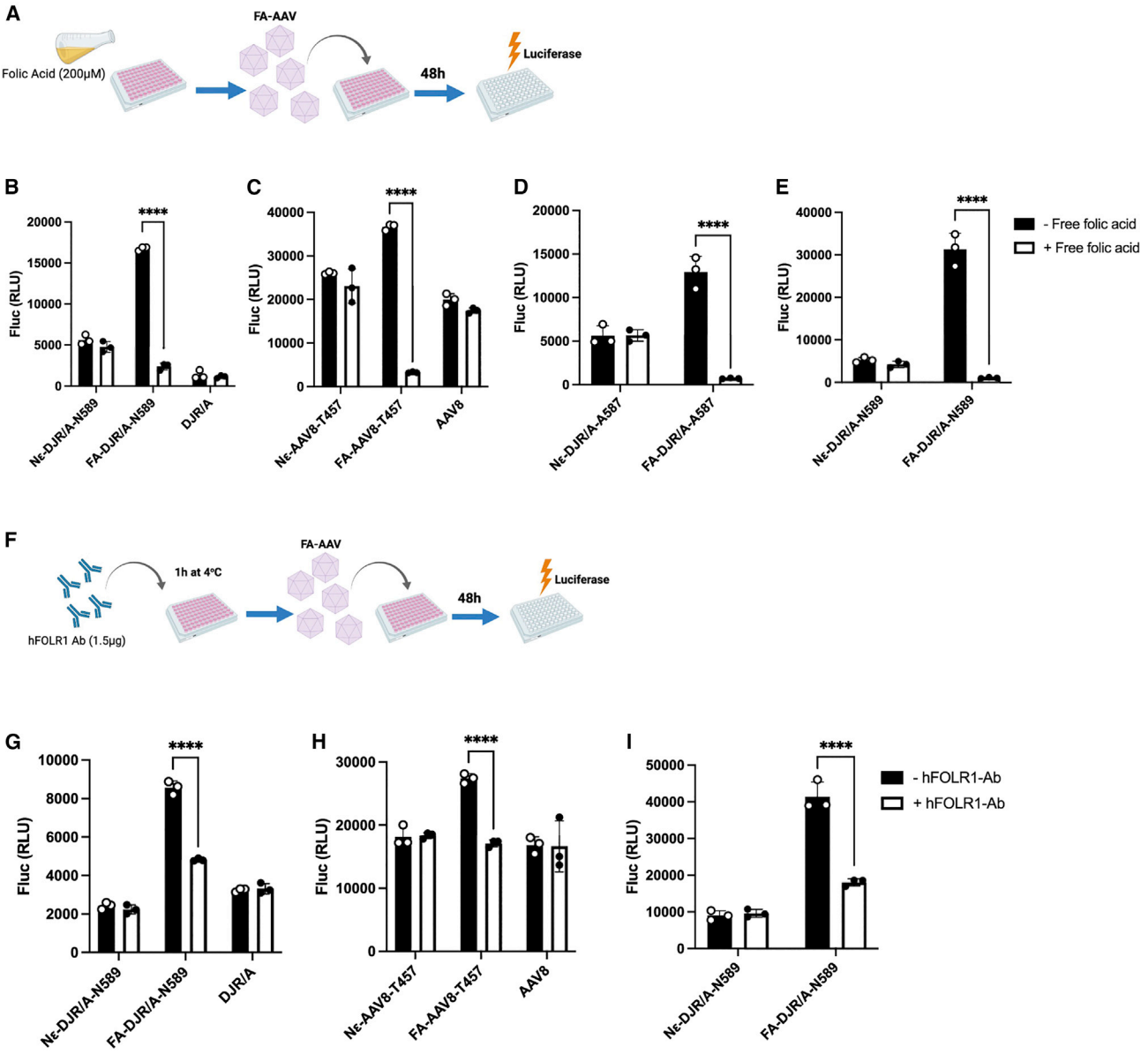

Figure 4. Evaluation of FA-AAV vector-specific uptake *in vitro*

(A) Schematic representation of the uptake assay conducted by adding 200 μM folic acid into the cell medium during AAV transduction. (B–D) Luciferase activity in HeLa cells transduced with (B) FA-DJR/A-N589, (C) FA-AAV8-T457, and (D) FA-DJR/A-A587. DJR/A, AAV8 and the unconjugated Nε-AAV vectors were used as controls. Folic acid (200 μM) was added into the cell medium at the time of AAV transduction (+free folic acid group). (E) Luciferase activity in MCF-7 cells transduced with FA-DJR/A-N589. DJR/A and the unconjugated Nε-AAV vectors were used as controls. Folic acid (200 μM) was added into the cell medium at the time of AAV transduction (+free folic acid group). (F) Schematic representation of the uptake assay conducted by pre-incubating the cells with the monoclonal anti-hFOLR1 antibody. (G and H) Luciferase activity in HeLa cells transduced with (G) FA-DJR/A-N589 and (H) FA-AAV8-T457. DJR/A, AAV8, and the unconjugated Nε-AAV vectors were used as controls. Cells were pre-incubated with an anti-hFOLR1 monoclonal antibody for 1 h at 4°C and then transduced with the AAV vectors (+hFOLR1-Ab group). (I) Luciferase activity in MCF-7 cells transduced with FA-DJR/A-N589. DJR/A and the unconjugated Nε-AAV vectors were used as controls. Cells were pre-incubated with an anti-hFOLR1 monoclonal antibody for 1 h at 4°C and then transduced with the AAV vectors (+hFOLR1-Ab group). Statistical analysis: (B–E, G–I) two-way ANOVA with Sidak's post hoc test; statistical significance was assumed with a p value of <0.05 (*), <0.01 (**), <0.001 (***), and <0.0001 (****). Error bars represent standard deviation.

For specific uptake assessment, we synthesized an antidote against the AS1411 aptamer and set up an *in vitro* assay to demonstrate the specificity of the AS1411-AAV transduction.[36] By treating the cells with different concentrations of the antidote, we predicted that transduction of AS1411-AAV would be inhibited along with the luciferase activity (Figure 5D). We used three different cancer cell lines, MCF-7,

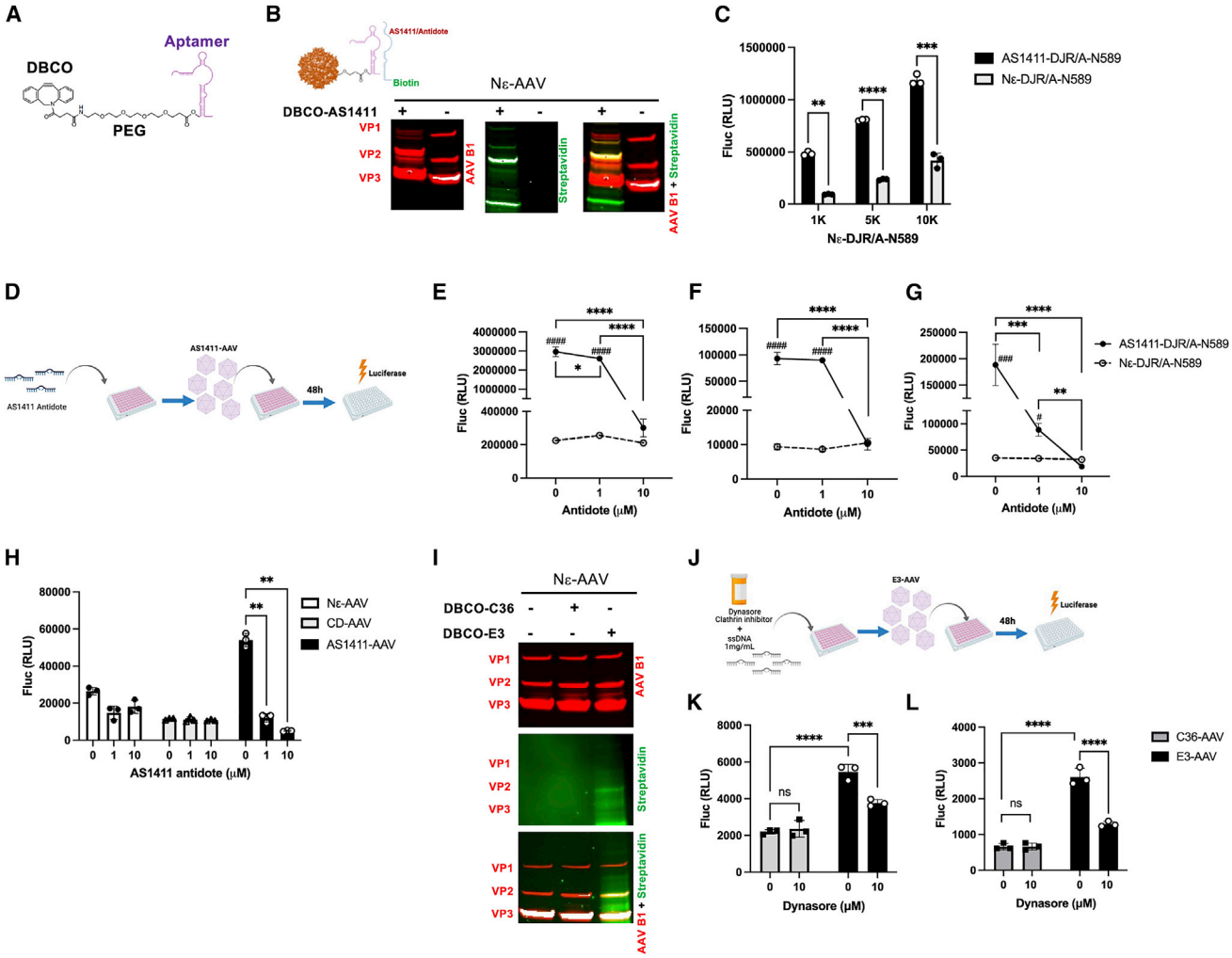

Figure 5. Characterization of DNA and RNA aptamers conjugated to Nε-AAV vectors

(A) Schematic representation of the DBCO-PEG-aptamer molecule. (B) Western blot analysis of Nε-AAV vector upon conjugation with DBCO-PEG-AS1411. An anti-AAV antibody, clone B1, was used to detect the VP1/2/3 capsid proteins of AAV. An anti-streptavidin antibody was used to detect the AS1411-conjugated Nε-AAV vector. (C) Luciferase activity in MCF-7 cells transduced with AS1411-DJR/A-N589 and the unconjugated Nε-DJR/A-N589 vectors at different MOI. (D) Schematic representation of the uptake assay conducted by incubating the cells with different concentrations of the AS1411 antidote. (E–G) Luciferase activity in (E) MCF-7, (F) A549, and (G) HeLa cells upon transduction with AS1411-DJR/A-N589. Unconjugated Nε-DJR/A-N589 vectors were used as controls. Cells were incubated with different concentrations of AS1411 antidote. (H) Luciferase activity in HeLa cells upon transduction with AS1411-DJR/A-A587. Unconjugated Nε-DJR/A-N589 and CD-DJR/A-A587 vectors were used as controls. Cells were incubated with different concentrations of AS1411 antidote. (I) Western blot analysis of Nε-AAV vector upon conjugation with DBCO-PEG-C36 or DBCO-PEG-E3. An anti-AAV antibody, clone B1, was used to detect the VP1/2/3 capsid proteins of AAV. An anti-streptavidin antibody was used to detect the specifically E3-conjugated Nε-AAV vector. (J) Schematic representation of the uptake assay conducted by incubating the cells with dynasore. (K and L) Luciferase activity in (K) Huh7 and (L) MCF-7 cells upon transduction with E3-DJR/A-A587. Unconjugated Nε-DJR/A-A587 and C36-DJR/A-A587 vectors were used as controls. Cells were incubated with 10 μM clathrin inhibitor, Dynasore. 0 μM AS1411-DJR/A-N589 = 3; 1 μM AS1411-DJR/A-N589 = 3; 10 μM AS1411-DJR/A-N589 = 3; 0 μM Nε-DJR/A-N589 = 3; 1 μM Nε-DJR/A-N589 = 3; 10 μM Nε-DJR/A-N589 = 3. Statistical analysis: (E–G, K, and L) two-way ANOVA with Sidak's post hoc test; (H) two-way ANOVA with Tukey's post hoc test. Statistical significance was assumed with p value of <0.05 (*), <0.01 (**), <0.001 (***), and <0.0001 (****) and with p value of <0.05 (#), <0.01 (##), <0.001 (###), and <0.0001 (####). Error bars represent standard deviation.

A549, and HeLa, which have been extensively employed for AS1411 aptamer characterization.[19] Notably, the luciferase activity from the AS1411-DJR/A-N589 was massively reduced at the dose of 10 μM antidote in all three cell lines, whereas the unconjugated Nε-DJR/A-N589 did not show any inhibition (Figures 5E–5G). In addition, we saw that as little as 1 μM antidote could partially inhibit the AS1411-DJR/A-N589 transduction in MCF-7 and even more clearly in HeLa cells (Figure 5G). Remarkably, in the absence of antidote, AS1411-AAV resulted in a significant 9-, 10-, and 5-fold increase in transduction compared with the unconjugated vector in MCF-7,

A549, and HeLa cells, respectively (Figures 5E–5G). Furthermore, the antidote significantly prevented the transduction of the other AS1411-DJR/A-A587 vector in both HeLa and MCF-7 cells (Figures S3B and S3C). Moreover, we conjugated Nε-AAV with a different aptamer,[37] originally isolated for the uptake in AML cells, which we called CD-AAV, to further demonstrate the specific nature of the AS1411-AAV uptake (Figure S3D). Indeed, HeLa cells infected with CD-AAV and in the presence of AS1411 antidote did not show any inhibition of transduction, similarly to the unconjugated Nε-AAV vector. In contrast, AS1411-AAV showed a dose-dependent decrease in luciferase activity (Figure 5H). AS1411 binding to cells has been shown to be blocked in the presence of salmon sperm DNA (ssDNA).[38] To this end, we treated both MCF-7 and A549 cells with 1 mg/mL ssDNA and transduced them with either the AS1411-DJR/A-N589 or its unconjugated counterpart, Nε-DJR/A-N589. The AS1411-DJR/A-N589 showed a massive ∼20-fold decrease of infectivity in cells treated with the ssDNA, while the unconjugated Nε-DJR/A-N589 displayed similar transduction levels in cells regardless of the ssDNA (Figures S3E and S3F). Taken together, transduction by AS1411-AAV is strictly dependent on the AS1411 aptamer regardless of the Nε-AAV capsid used similarly to FA receptor-dependent FA-AAV transduction.

To further demonstrate the versatility of this system beyond the use of DNA aptamers, we conjugated the AAV with the E3 RNA aptamer.[22] This aptamer has been reported to specifically target various tumor cells[23] and was successfully conjugated with anti-cancer drugs to treat prostate cancer using a xenograft mouse model.[22] To this end, upon vector conjugation, we probed the western blot membrane with a biotinylated E3 oligonucleotide antidote. Similar to the DNA aptamer conjugation, we showed that the E3 aptamer is specifically conjugated to the AAV. In contrast, both the unconjugated and the C36, non-specific control RNA aptamer-conjugated vectors did not show any specific signal when incubated with the E3-specific probe (Figure 5I). *In vitro* assessment of E3-AAV showed a significantly enhanced transduction in liver hepatoma cells compared with the unconjugated Nε-AAV or the C36-AAV vectors (Figure S3G). To quickly evaluate the E3-specific uptake *in vitro*, we incubated the cells with the clathrin inhibitor dynasore, known to inhibit E3 uptake[22] (Figure 5J). The E3-AAV uptake was significantly inhibited by treating Huh7 (Figure 5K) and MCF-7 (Figure 5L) cells with dynasore, whereas the C36-AAV control vector was not inhibited. Interestingly, the addition of ssDNA onto cells to block non-specific charged-based aptamer binding was able to inhibit the uptake of the AS1411-AAV vector (Figures S3E and S3F) but not of the E3-AAV vector.

Highly specific targeting of FA-AAV and AS1411-AAV vectors *in vivo*

To evaluate the Nε-AAV vectors *in vivo*, we firstly needed to improve their yield. Previously, researchers have found that the CAG promoter element in the AAV cassette might negatively impact AAV production as a result of vector genome truncation.[39] This prompted us to replace the large CAG promoter with a newly characterized small ubiquitous promoter, INS84.[40] The new Nε-AAV expressing firefly luciferase under the small INS84 promoter resulted in significantly higher vector titers compared with the AAV cassette carrying the CAG promoter (Figure S4A).

Moreover, we conjugated the Nε-DJR/A-A587 (Nε-AAV hereafter) containing the INS84-Fluc cassette with either folic acid (FA-AAV) or the AS1411 aptamer (AS1411-AAV) and tested them in HeLa cells. FA-AAV and AS1411-AAV resulted in significantly higher luciferase activity compared with their unconjugated counterparts but with similar activity compared with the Nε-AAV containing the CAG promoter (Figures S4B and S4C).

To assess these new Nε-AAV vectors *in vivo*, we subcutaneously transplanted HeLa cells into immunodeficient nude mice and subcutaneously injected the AAV vectors once the HeLa cells had formed palpable tumors. The luciferase expression of the unconjugated Nε-AAV, FA-AAV, and AS1411-AAV vectors was assessed 3, 7, and 14 days after AAV treatment by *in vivo* imaging (Figure 6A). All three vectors, Nε-AAV, FA-AAV, and AS1411-AAV, were able to infect the tumor cells, and by day 14 reached maximal expression, albeit expression was detectable at earlier time points (Figures 6B, S4D, and S4E). Nε-AAV and FA-AAV displayed a slightly higher luciferase signal in tumor cells compared with AS1411-AAV (Figure 6C). However, a major difference was the off-target expression in the liver, with Nε-AAV exhibiting the most luciferase activity, followed by FA-AAV, and finally AS1411-AAV, which did not show any activity in the liver (Figures 6D and 6E).

Interestingly, luciferase measurement in the harvested tissues 14 days after the AAV treatment confirmed that the liver was transduced by the Nε-AAV and FA-AAV vectors but not by the AS1411-AAV vector. Conversely, we did not see any significant difference in luciferase activity on the explanted tumor cells among the mice treated with Nε-AAV, FA-AAV, and AS1411-AAV vectors (Figure S4F).

These results corroborated *in vivo* our previous *in vitro* findings demonstrating the cell-specific transduction of FA-AAV and AS1411-AAV.

DISCUSSION

Recently, the gene therapy field has seen a massive increase in the development of novel AAV capsids.[4] However, AAV vectors can still result in off-target transduction and, when used at high doses, raise the risk of acute AAV-related toxicity[41–43] (https://www.fda.gov/media/151969/download). Thus, designing vectors able to transduce specific cells and at the same time minimize their off-target uptake is still an unmet medical need in the context of AAV *in vivo* gene transfer. In this study we developed new chemically engineered AAVs, which could be programmed by single-molecule conjugation to retarget vector tropism toward specific cells.

We pursued different strategies to incorporate the unnatural amino acid onto the AAV capsid, by (1) introducing the modification in

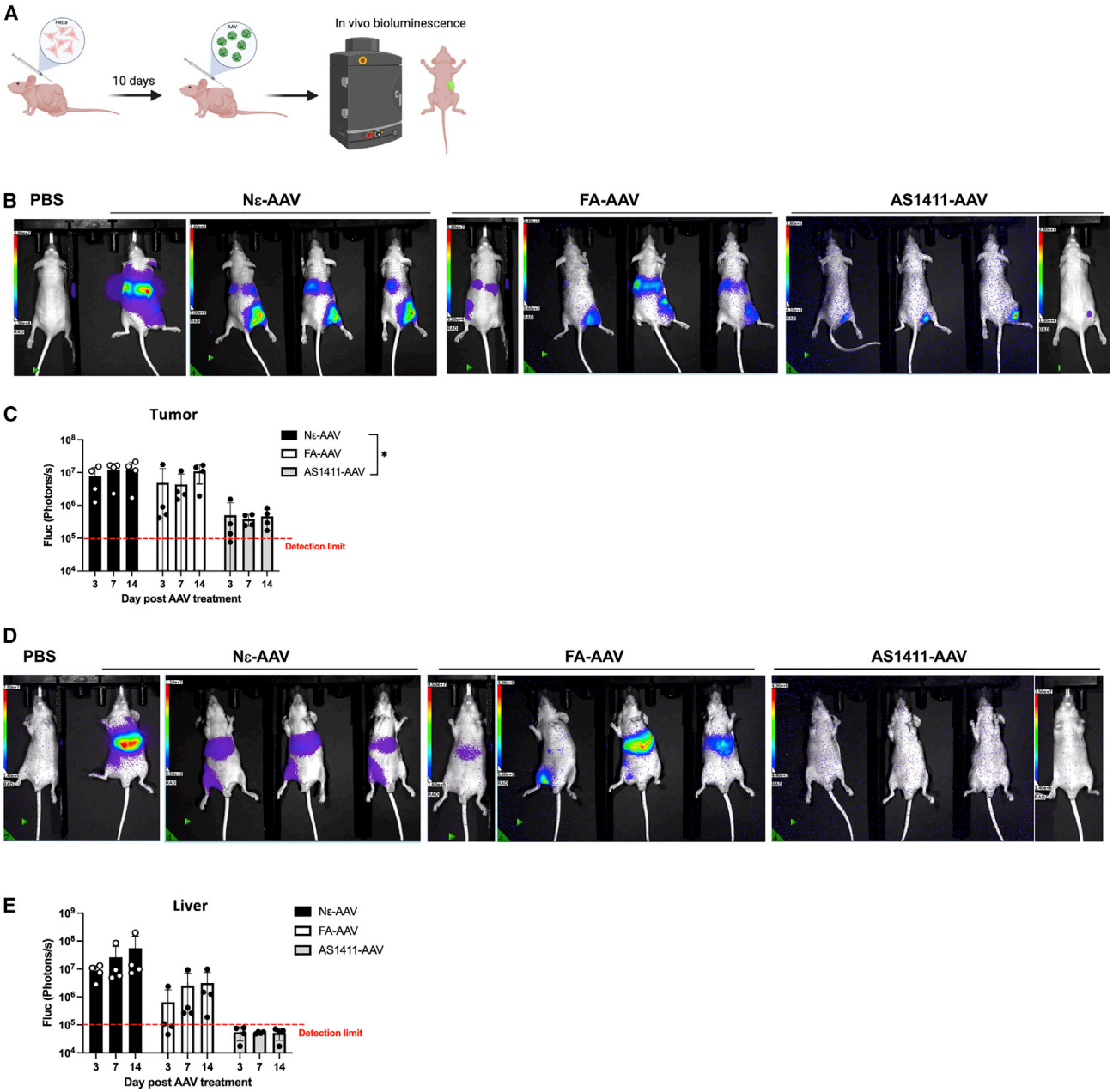

Figure 6. *In vivo* characterization of FA-AAV and AS1411-AAV vectors

(A) Schematic representation of the *in vivo* study. (B) Dorsal image of mice treated with 5×10^9 vg of Nε-AAV, FA-AAV, and AS1411-AAV 14 days after AAV treatment. PBS-injected mouse was used as negative control. (C) Luciferase signal from tumor of mice treated with 5×10^9 vg of Nε-AAV, FA-AAV, and AS1411-AAV at 3, 7, and 14 days after AAV treatment. (D) Ventral image of mice treated with 5×10^9 vg of Nε-AAV, FA-AAV, and AS1411-AAV 14 days after AAV treatment. PBS-injected mouse was used as negative control. (E) Luciferase signal from liver of mice treated with 5×10^9 vg of Nε-AAV, FA-AAV, and AS1411-AAV at 3, 7, and 14 days after AAV treatment. Statistical analysis: (C and E) two-way ANOVA with Tukey's post hoc test; statistical significance was assumed with p value of <0.05 (*), <0.01 (**), <0.001 (***), and <0.0001 (****). Error bars represent standard deviation.

all three VP capsid proteins and (2) inserting the unnatural amino acid only on the VP2[29] or VP3[30] proteins. Nevertheless, the latter approach resulted in a significant reduction of vector infectivity. This might occur as a result of the low efficiency of modified VP2 and VP3 complementation when provided in *trans* during the vector production. In this case, the final AAV preparation might possibly

contain particles devoid of either VP2 or VP3 protein, which is known to result in reduced AAV transduction.[44–46]

Despite the fact that we do not know the exact number of capsid VP proteins that have been successfully conjugated in our vector preparation, the data *in vitro* and *in vivo* clearly supported the view that the ligand-vector conjugation was able to specifically modify the AAV tropism.

The other important parameter we learned was that placement of the unnatural amino acid within the capsid affects both AAV production and transduction efficiency, while transduction efficiency was also dependent on the size of the linker.

Biorthogonal copper-free click chemistry[28] for AAV conjugation has been successfully exploited to label the capsid with fluorophores in order to track the vector in live cells,[47] and different chemical moieties have been utilized in an attempt to shield the vector from anti-AAV antibodies.[48]

To date, only two groups reported the use of AAV2 unnatural amino acid-modified vectors *in vivo*, both using the RGD-derived peptides as the ligand.[49,50] However, the AAV2 yield is significantly low, and large-scale production might prove to be challenging.[51] Katrekar et al. recently demonstrated that the use of AAV-DJ led to a significant improvement of vector titers compared with AAV2.[52] In our study, to further improve the vector production, we replaced the regulatory elements within the AAV expression cassette. Of note, for the subsequent vector conjugation in their study Katrekar et al. employed copper as catalyst for the click chemistry reaction, whereas we used a copper-free cycloaddition reaction reported to be more suitable for use in living systems.[28]

Tumor cells usually undergo genomic and metabolic dysregulation, which leads to the expression of tumor-specific cellular surface molecules. Hence, researchers have been trying to develop ligands to specifically target cancer cells.[53] To this end, folic acid and aptamers have been conjugated to drugs, nucleic acids, and lipid nanoparticles.[13,17] Nevertheless, nanoparticles have been associated with acute cell toxicity depending on their formulation.[54,55] Moreover, like most oligonucleotides, aptamers possess very poor and limited endosomal escape[56] that may hamper their development as therapeutics. By contrast, AAV vectors use their intrinsic phospholipase A_2 activity, which allows their effective release from the endosomal compartment and very efficient nuclear trafficking.[57]

To our knowledge, this is the first study to show the successful conjugation of aptamers to AAV capsids in order to efficiently enhance and redirect their tropism. We have characterized, through a series of *in vitro* uptake assays and the use of different cell lines, the transduction specificity of AAV conjugated to a peptide molecule (FA), an RNA aptamer (E3), and a DNA aptamer (AS1411). We have also shown that the ligand's characteristics are transferable, since the Nε-AAV serotype did not influence the vector uptake.

In vivo study in a xenograft animal model demonstrated that FA-AAVs and AS1411-AAVs can be efficiently and specifically taken up by tumor cells, unlike the unconjugated vector which showed off-target expression in liver. Nevertheless, the FA-AAV liver transduction in some animals could likely be due to the ectopic expression of folic acid receptors on the surface of murine hepatocytes.

One of the limitations of this study could be the lower yield of Nε-AAVs compared with their wild-type counterparts. However, engineering the producer cells to constitutively express the prokaryotic tRNA/tRNA synthases,[58,59] combined with the discovery of novel orthogonal tRNA/tRNA synthases that possess an enhanced ability to incorporate unnatural amino acids,[60,61] might dramatically improve the manufacture of Nε-AAVs.

The use of aptamers to modulate AAV tropism presents apparent advantages: (1) large-scale production of nucleic acids is less expensive than protein- or antibodies-based drugs;[62] (2) the possible use of a universal vector will further reduce the costs of manufacture; (3) the aptamer selection for a specific type of cells is more simple than screening libraries of antibodies or AAVs; and (4) chemical synthesis of oligonucleotides facilitates straightforward attachment of moieties that support their subsequent conjugation to the modified AAV capsids described herein.

Recently, aptamer selection has been expanded *in vivo* through direct injection of nucleic acid-based libraries in animal models.[63–65] Moreover, organs-on-chip technology[66] and organoids[67,68] could be valuable resources for the isolation of specific aptamers for human cells. These advances in combination with machine learning have allowed researchers to predict and optimize an aptamer sequence with an improved affinity for the desired target protein.[69] A further evolution of this approach could be the use of AlphaFold for precise protein structure prediction[70,71] which, in the future, might pave the way for a total *in silico* design of aptamers that bind specific cell-surface receptors.

Eventually, the chemically modified Nε-AAV combined with wider aptamer versatility could create a novel class of easily programmable vectors, which might help us move toward the goal of new cell-type-specific vectors.

MATERIALS AND METHODS

Plasmid construction

All plasmids generated in this study have been produced by Gibson assembly using NEBuilder HiFi DNA Assembly Master Mix (NEB, catalog number [#]E2621S). Single-nucleotide mutations were introduced by a QuickChange II Site-Directed Mutagenesis Kit (Agilent Technologies, #200523). A pcDNA3.1 plasmid backbone was used for the expression of VP2 or VP3 under the control of a cytomegalovirus promoter. The pAcBac1.tR4-MbPyl plasmid was a gift from Peter Schultz (Addgene plasmid, #50832).[27] The pAAV plasmid with the ubiquitous CAG promoter

upstream of the firefly luciferase transgene for the *in vitro* experiments was generated in the Kay lab and available at Addgene (#83281). For the *in vivo* studies the CAG promoter was swapped with the minimal ubiquitous INS84 promoter kindly provided by Marcus Grompe.[40]

Nε-AAV vector production and titration

Cell transfection for AAV production was performed as previously reported[72] with few modifications. In brief, the N^{ϵ}-2-azidoethyloxycarbonyl-L-lysine (Toronto Research, #A848920) was added to the transfection medium at the final concentration of 1.5 mM for the Nε-AAV production. Transfection was carried out using the following plasmids: pRep/Cap (5 μg/225 cm^2 flask), pXX6-Ad5 (10 μg/225 cm^2 flask), pAAV plasmid with the gene of interest (5 μg/225 cm^2 flask), and pAcBac1.tR4-MbPyl (10 μg/225 cm^2 flask). The AAV vectors were purified using the AAVpro Purification Kit (Takara, #6666) following the manufacturer instructions. For crude lysate AAVs, the cells were harvested and underwent three cycles of freeze-thaw for lysis. They were spun at 5,000 × *g* at 4°C for 15 min to pellet cell debris. Supernatant was collected and treated with 1 μL of benzonase for 1 h at 37°C. Cells were spun at 5,000 × *g* for 10 min to pellet debris and the supernatant collected. The supernatant was incubated for 1 h at 4°C in ice. Another centrifugation step at 7,000 × *g* at 4°C for 30 min was carried out. Supernatant was collected and stored at −80°C until the day of AAV transduction.

Vector titers were obtained by qPCR on the CFSX384 instrument (Bio-Rad) using Brilliant III Ultra-Fast SYBR QPCR MM (Agilent, #600882).

Primers: forward (luciferase) 5′- ctt cga ggc taa ggt ggt gg-3′; reverse (luciferase) 5′-tcg ggg ttg tta acg tag cc-3′.

DBCO chemicals preparation and AAV conjugation

Nε-AAVs were conjugated with the DBCO-PEG folic acid or DBCO-PEG biotin (NANOCS, #PG2-DBFA, #PG2-BNDB). DBCO-PEG chemicals were resuspended in 20% DMSO to a final concentration of 2 mM used as stock solution. Before the click reaction, the stock was further diluted to 500 mM in 20% DMSO solution. DBCO-PEG moieties were added to Nε-AAV to a final concentration of 100 mM and incubated overnight on a tube rotor at 4°C. The Nε-AAV unconjugated control vectors were incubated in the same 20% DMSO solution used for the DBCO-PEG solubilization. DBCO-PEG-Aptamer preparation was carried out as previously reported.[73] In brief, the DNA aptamers, AS1411 and CD, carrying an amino (NH_2) modified 5′ end, were synthesized from Integrated DNA Technology:

AS1411: 5′-5AmMC6-TTT TTT TTT TTT GGT GGT GGT GGT GTT GGT GGT GGT GG-3′.

CD: 5′-5AmMC6-TTT TTT TTT TTT GGG GCC GGG GCA AGG GGG GGG TAC CGT GGT AGG AC-3′.

The E3 and C36 RNA aptamers were synthesized as previously reported.[22] In brief, the E3 (GGC UUU CGG GCU UUC GGC AAC AUC AGC CCC UCA GCC) and C36 (GGC GUA GUG AUU AUG AAU CGU GUG CUA AUA CAC GCC) aptamers were synthesized by solid-phase synthesis on a MerMade 12 Synthesizer (Biosearch Technologies), as previously described.[74] The aptamers were synthesized using 2′-F-modified pyrimidines and 2′OH purines on an inverted dT CPG column. Synthesis reagents were purchased from Glen Research (Sterling, VA) and Chemgenes (Wilmington, MA). All aptamers were synthesized bearing a 5′ amine using a C6 phosphoramidite (Glen Research, Sterling, VA).

The aptamers were incubated with DBCO-PEG4-NHS Ester (Click Chemistry Tool, #A134-10) at room temperature for 2 h. The resulting DBCO-PEG-aptamer was finally purified using Cytiva Illustra MicroSpin G-25 columns (Cytiva Life Sciences, #27532501) following the manufacturer's instructions. DBCO-PEG-Aptamer was added to the Nε-AAVs to a final concentration of 125 μM and incubated overnight on a tube rotor at 4°C.

The conjugated AAVs, both aptamer- and FA-conjugated, were dialyzed using Amicon Ultra-0.5 Centrifugal Filter Unit 100k (Sigma, #UFC510024). The columns were washed by centrifugation at 10,000 × *g* for 10 min at 4°C using 450 μL of PBS-0.0001% Pluronic F-68 (Pluronic F-68 Polyol, 100 mL, MP Biomedicals, Fisher, #ICN2750049). The conjugated AAV was added to 450 μL of PBS-0.0001% Pluronic F-68 and washed three times with 450 μL of PBS-0.0001% Pluronic F-68 solution by three centrifugations at 10,000 × *g* for 10 min at 4°C. After the last washing step, the conjugated AAV was transferred into a new 1.5-mL sterile tube.

Silver stain analysis of AAV vectors was performed using SYPRO Ruby Protein Gel Stain (Thermo Fisher, #S12000) following the manufacturer's instructions.

Cell lines

The cells used for the folic acid experiments were grown in RPMI 1640 medium (Fisher, #27016021) supplemented with 10% fetal bovine serum (FBS) and 100 IU/mL penicillin/streptomycin. The rest of the experiments were carried out using DMEM (Thermo Fisher, #15017CV) supplemented with 10% FBS, 2 mM L-glutamine, and 100 IU/mL penicillin/streptomycin. All the cells were maintained in a humidified incubator at 37°C with 5% CO_2. Total mRNA was extracted from HeLa, MCF-7, and A549 using an RNeasy mini kit (QIAGEN) following the manufacturer's instructions. mRNA was converted to cDNA using a Maxima First Strand cDNA Synthesis Kit for qRT-PCR (Thermo Fisher, #K1671).

qPCR was performed in the CFSX384 instrument (Bio-Rad) using Brilliant III Ultra-Fast SYBR QPCR MM (Agilent, #600882).

Primers: forward (hFOLR1) 5′-aca agg att gca tgg gcc ag-3′; reverse (hFOLR1) 5′-agg tgc cat ctc tcc aca gtg-3′; forward (hACTB) 5′-gtc

acc aac tgg gac gac at-3′; reverse (hACTB) 5′-gta cat ggc tgg ggt gtt ga-3′.

AAV transduction

Cells were incubated with AAV vectors for 48 h using an MOI of 5,000 unless specified otherwise in the figure legends. Cell lysis and luciferase assay were performed using the Promega Luciferase 1000 Assay System (Promega, #E4550) following the manufacturer's instructions. For the uptake experiments, 1.5 μg per well of anti-hFOLR1 antibody (Thermo Fisher, #MA5-23917), 200 μM/well of folic acid (Sigma, #F8758-25G), 1 mg/mL per well of ssDNA (Sigma, #262,012-1GM), 10 μM/well of the clathrin inhibitor dynasore hydrate (MilliporeSigma, #D7693-5MG), and different concentrations of AS1411 aptamer antidote (sequence 5′-CCA CCA CCA CCA CAA CCA CC-3′) acquired from Integrated DNA Technology, were used.

Western blot

AAV samples were loaded on a 4%–15% gradient polyacrylamide gel (Fisher, #34028). Protein transfer was performed using the iBlot system (Thermo Fisher, #IB23002). The membrane was blocked with Odyssey buffer (Fisher, #NC0730870) and incubated with the anti-AAV antibody (Gene Tex, #GTX44495) or a streptavidin-conjugated antibody (Fisher, #NC9386176), both diluted 1:1,000 in Odyssey buffer. The membrane was washed and incubated with a secondary antibody (Fisher, #92532210) diluted 1:100,000 and visualized by the Odyssey imaging system (Li-Cor Biosciences). For AAV-aptamer detection, the membrane, after the blocking step, was incubated with 1 μM AS1411-(5′-CCA CCA CCA CCA CAA CCA CCA CCA CC-biotin-3′), CD-(5′-CCC CCC ATG GCA CCA TCC TG-biotin-3′), and E3-(5′-GAT GTT GCC GAA AGC CCG AA-biotin-3′) probes overnight at room temperature, and subsequently incubated with a streptavidin-conjugated antibody for 2 h at room temperature (Fisher, #NC9386176).

Transmission electron microscopy

The AAV vectors were placed on a 300-mesh carbon/formvar-coated Cu grid and allowed to settle for 3 min. Samples were washed two times with MilliQ-H_2O and stained for 1 min with 1% uranyl acetate in mQ-H_2O. AAV samples were allowed to dry. Image acquisition was performed on a JEOL-JEM1400 microscope at 120 kV.

In vivo study

Mouse experiments were conducted and approved by the Administrative Panel on Laboratory Animal Care of Stanford University. Nude mice (NU/J) were acquired from The Jackson Laboratory (#002019). The animals were kept in the animal facility with a normal night/day cycle and on autoclaved chow *ad libitum*. HeLa cells were grown in 225-cm^2 flasks at ∼90% confluence and >90% viability before transplantation. On the day of transplantation, cells were harvested and resuspended in PBS. Cells (5×10^6) were injected subcutaneously in the animal flank in 200 μL of sterile PBS. AAV injections were performed subcutaneously using 5×10^9 vector genomes/mouse. *In vivo* luciferase imaging was performed using the Lago optimal imaging system (Spectral Instruments Imaging). Luciferase images were analyzed using Aura Software (Spectral Instruments Imaging). Explanted liver and HeLa tumor were freshly homogenized in PBS using a Bullet Blender (Next Advance). The luciferase assay was performed using the Promega Luciferase 1000 Assay System (Promega, #E4550) following the manufacturer's instructions. Protein concentration in tissue samples was measured with a Pierce BCA protein assay kit (Thermo Fisher, #23227) following the manufacturer's instructions.

Statistics

GraphPad Prism was used for statistical analysis. Datasets were compared by ANOVA with a proper post hoc correction (see figure legends). Statistical significance was assumed with p values of <0.05 (* or #), <0.01(** or ##), <0.001 (*** or ###), and <0.0001 (**** or ####). Bars in graphs represent standard deviation for each group.

DATA AVAILABILITY

All data generated for this study are included in this published manuscript and relative supplemental information.

SUPPLEMENTAL INFORMATION

Supplemental information can be found online at https://doi.org/10.1016/j.omtn.2023.01.007.

ACKNOWLEDGMENTS

We acknowledge the Markus Grompe lab for the plasmid containing the INS84 promoter sequence. We would like to thank the Stanford Center for Innovation in *In Vivo* Imaging (Sci3) small animal imaging center for the *in vivo* luciferase study; we thank the Cell Sciences Imaging Facility and Ruth Yamawaki for the assistance on the preparation and acquisition of the electron microscopy images. Figures 1A, 2A–2C, 4A, 4F, 5B, 5D, 5L, and 6A were made using BioRender. The project described was supported by National Institutes of Health (NIH) R01 AI116698 (M.A.K.) and in part by NIH S10 award number 1S10OD028536-01, titled "OneView 4kX4k sCMOS camera for transmission electron microscopy applications" from the Office of Research Infrastructure Programs. RNA aptamer synthesis and purification was supported by UG3 TR002852 (B.A.S.). The contents are solely the responsibility of the authors and do not necessarily represent the official views of the National Center for Research Resources or the NIH.

AUTHOR CONTRIBUTIONS

F.P. and C.Z. designed and performed the FA-AAV *in vitro* experiments. F.P. designed and performed the rest of the *in vitro* experiments. F.P. and F.Z. conducted the animal studies. B.P.G. and B.A.S. synthesized the RNA aptamers E3/C36 and provided insightful discussions about the aptamer studies. F.P. and M.A.K. conceived the project, provided intellectual feedback throughout the project, and wrote the manuscript.

DECLARATION OF INTERESTS

The authors declare no competing interests.

REFERENCES

1. Kuzmin, D.A., Shutova, M.V., Johnston, N.R., Smith, O.P., Fedorin, V.V., Kukushkin, Y.S., van der Loo, J.C.M., and Johnstone, E.C. (2021). The clinical landscape for AAV gene therapies. Nat. Rev. Drug Discov. *20*, 173–174. https://doi.org/10.1038/D41573-021-00017-7.
2. Mendell, J.R., Al-Zaidy, S.A., Rodino-Klapac, L.R., Goodspeed, K., Gray, S.J., Kay, C.N., Boye, S.L., Boye, S.E., George, L.A., Salabarria, S., et al. (2021). Current clinical applications of in vivo gene therapy with AAVs. Mol. Ther. *29*, 464–488. https://doi.org/10.1016/J.YMTHE.2020.12.007.
3. Li, C., and Samulski, R.J. (2020). Engineering adeno-associated virus vectors for gene therapy. Nat. Rev. Genet. *21*, 255–272. https://doi.org/10.1038/S41576-019-0205-4.
4. Wang, D., Tai, P.W.L., and Gao, G. (2019). Adeno-associated virus vector as a platform for gene therapy delivery. Nat. Rev. Drug Discov. *18*, 358–378. https://doi.org/10.1038/S41573-019-0012-9.
5. Lugin, M.L., Lee, R.T., and Kwon, Y.J. (2020). Synthetically engineered adeno-associated virus for efficient, safe, and versatile gene therapy applications. ACS Nano *14*, 14262–14283. https://doi.org/10.1021/ACSNANO.0C03850.
6. Lam, A.K., Frabutt, D., Li, L., and Xiao, W. (2021). Chemical modifications of the capsid for redirecting and improving the efficacy of adeno-associated virus vectors. Hum. Gene Ther. *32*, 1433–1438. https://doi.org/10.1089/hum.2021.124.
7. de la Torre, D., and Chin, J.W. (2021). Reprogramming the genetic code. Nat. Rev. Genet. *22*, 169–184. https://doi.org/10.1038/s41576-020-00307-7.
8. Italia, J.S., Zheng, Y., Kelemen, R.E., Erickson, S.B., Addy, P.S., and Chatterjee, A. (2017). Expanding the genetic code of mammalian cells. Biochem. Soc. Trans. *45*, 555–562. https://doi.org/10.1042/BST20160336.
9. Sun, S.B., Schultz, P.G., and Kim, C.H. (2014). Therapeutic applications of an expanded genetic code. Chembiochem *15*, 1721–1729. https://doi.org/10.1002/CBIC.201402154.
10. Kelemen, R.E., Erickson, S.B., and Chatterjee, A. (2018). Production and chemoselective modification of adeno-associated virus site-specifically incorporating an unnatural amino acid residue into its capsid. Methods Mol. Biol. *1728*, 313–326. https://doi.org/10.1007/978-1-4939-7574-7_20.
11. Mével, M., Bouzelha, M., Leray, A., Pacouret, S., Guilbaud, M., Penaud-Budloo, M., Alvarez-Dorta, D., Dubreil, L., Gouin, S.G., Combal, J.P., et al. (2019). Chemical modification of the adeno-associated virus capsid to improve gene delivery. Chem. Sci. *11*, 1122–1131. https://doi.org/10.1039/C9SC04189C.
12. Liu, Y., Fang, Y., Zhou, Y., Zandi, E., Lee, C.L., Joo, K.I., and Wang, P. (2013). Site-specific modification of adeno-associated viruses via a genetically engineered aldehyde tag. Small *9*, 421–429. https://doi.org/10.1002/SMLL.201201661.
13. Fernández, M., Javaid, F., and Chudasama, V. (2018). Advances in targeting the folate receptor in the treatment/imaging of cancers. Chem. Sci. *9*, 790–810. https://doi.org/10.1039/C7SC04004K.
14. Gangopadhyay, S., Nikam, R.R., and Gore, K.R. (2021). Folate receptor-mediated siRNA delivery: recent developments and future directions for RNAi therapeutics. Nucleic Acid Ther. *31*, 245–270. https://doi.org/10.1089/nat.2020.0882.
15. Ebrahimnejad, P., Sodagar Taleghani, A., Asare-Addo, K., and Nokhodchi, A. (2022). An updated review of folate-functionalized nanocarriers: a promising ligand in cancer. Drug Discov. Today *27*, 471–489. https://doi.org/10.1016/J.DRUDIS.2021.11.011.
16. Le, Q., Loeb, K.R., and Meshinchi, S. (2022). CBFA2T3-GLIS2 Model of Pediatric Acute Megakaryoblastic Leukemia Identifies FOLR1 as a CAR T Cell Target.
17. Shigdar, S., Schrand, B., Giangrande, P.H., and de Franciscis, V. (2021). Aptamers: cutting edge of cancer therapies. Mol. Ther. *29*, 2396–2411. https://doi.org/10.1016/J.YMTHE.2021.06.010.
18. Poolsup, S., and Kim, C.Y. (2017). Therapeutic applications of synthetic nucleic acid aptamers. Curr. Opin. Biotechnol. *48*, 180–186. https://doi.org/10.1016/j.copbio.2017.05.004.
19. Tong, X., Ga, L., Ai, J., and Wang, Y. (2022). Progress in cancer drug delivery based on AS1411 oriented nanomaterials. J. Nanobiotechnology *20*, 57. https://doi.org/10.1186/s12951-022-01240-z.
20. Bates, P.J., Reyes-Reyes, E.M., Malik, M.T., Murphy, E.M., O'Toole, M.G., and Trent, J.O. (2017). G-quadruplex oligonucleotide AS1411 as a cancer-targeting agent: uses and mechanisms. Biochim. Biophys. Acta. Gen. Subj. *1861*, 1414–1428. https://doi.org/10.1016/j.bbagen.2016.12.015.
21. Mongelard, F., and Bouvet, P. (2010). AS-1411, a guanosine-rich oligonucleotide aptamer targeting nucleolin for the potential treatment of cancer, including acute myeloid leukemia. Curr. Opin. Mol. Ther. *12*, 107–114.
22. Powell Gray, B., Kelly, L., Ahrens, D.P., Barry, A.P., Kratschmer, C., Levy, M., and Sullenger, B.A. (2018). Tunable cytotoxic aptamer–drug conjugates for the treatment of prostate cancer. Proc. Natl. Acad. Sci. USA *115*, 4761–4766. https://doi.org/10.1073/pnas.1717705115.
23. Powell Gray, B., Song, X., Hsu, D.S., Kratschmer, C., Levy, M., Barry, A.P., and Sullenger, B.A. (2020). An aptamer for broad cancer targeting and therapy. Cancers *12*, 3217. https://doi.org/10.3390/cancers12113217.
24. Grimm, D., Lee, J.S., Wang, L., Desai, T., Akache, B., Storm, T.A., and Kay, M.A. (2008). In vitro and in vivo gene therapy vector evolution via multispecies interbreeding and retargeting of adeno-associated viruses. J. Virol. *82*, 5887–5911. https://doi.org/10.1128/JVI.00254-08.
25. Perabo, L., Goldnau, D., White, K., Endell, J., Boucas, J., Humme, S., Work, L.M., Janicki, H., Hallek, M., Baker, A.H., et al. (2006). Heparan sulfate proteoglycan binding properties of adeno-associated virus retargeting mutants and consequences for their in vivo tropism. J. Virol. *80*, 7265–7269. https://doi.org/10.1128/JVI.00076-06.
26. Lerch, T.F., O'Donnell, J.K., Meyer, N.L., Xie, Q., Taylor, K.A., Stagg, S.M., and Chapman, M.S. (2012). Structure of AAV-DJ, a retargeted gene therapy vector: cryo-electron microscopy at 4.5 Å resolution. Structure *20*, 1310–1320. https://doi.org/10.1016/J.STR.2012.05.004.
27. Chatterjee, A., Xiao, H., Bollong, M., Ai, H.W., and Schultz, P.G. (2013). Efficient viral delivery system for unnatural amino acid mutagenesis in mammalian cells. Proc. Natl. Acad. Sci. USA *110*, 11803–11808. https://doi.org/10.1073/pnas.1309584110.
28. Agard, N.J., Prescher, J.A., and Bertozzi, C.R. (2004). A strain-promoted [3 + 2] azide-alkyne cycloaddition for covalent modification of biomolecules in living systems. J. Am. Chem. Soc. *126*, 15046–15047. https://doi.org/10.1021/ja044996f.
29. Münch, R.C., Janicki, H., Völker, I., Rasbach, A., Hallek, M., Büning, H., and Buchholz, C.J. (2013). Displaying high-affinity ligands on adeno-associated viral vectors enables tumor cell-specific and safe gene transfer. Mol. Ther. *21*, 109–118. https://doi.org/10.1038/mt.2012.186.
30. Feiner, R.C., Teschner, J., Teschner, K.E., Radukic, M.T., Baumann, T., Hagen, S., Hannappel, Y., Biere, N., Anselmetti, D., Arndt, K.M., et al. (2019). RAAV engineering for capsid-protein enzyme insertions and mosaicism reveals resilience to mutational, structural and thermal perturbations. Int. J. Mol. Sci. *20*, 5702. https://doi.org/10.3390/ijms20225702.
31. Yu, Y., Wang, J., Kaul, S.C., Wadhwa, R., and Miyako, E. (2019). Folic acid receptor-mediated targeting enhances the cytotoxicity, efficacy, and selectivity of withania somnifera leaf extract: in vitro and in vivo evidence. Front. Oncol. *9*, 602. https://doi.org/10.3389/FONC.2019.00602.
32. Nam, H.-J., Lane, M.D., Padron, E., Gurda, B., McKenna, R., Kohlbrenner, E., Aslanidi, G., Byrne, B., Muzyczka, N., Zolotukhin, S., et al. (2007). Structure of adeno-associated virus serotype 8, a gene therapy vector. J. Virol. *81*, 12260–12271. https://doi.org/10.1128/JVI.01304-07.
33. Lee, G.K., Maheshri, N., Kaspar, B., and Schaffer, D.V. (2005). PEG conjugation moderately protects adeno-associated viral vectors against antibody neutralization. Biotechnol. Bioeng. *92*, 24–34. https://doi.org/10.1002/bit.20562.
34. Nimjee, S.M., White, R.R., Becker, R.C., and Sullenger, B.A. (2017). Aptamers as therapeutics. Annu. Rev. Pharmacol. Toxicol. *57*, 61–79. https://doi.org/10.1146/ANNUREV-PHARMTOX-010716-104558.
35. Soundararajan, S., Chen, W., Spicer, E.K., Courtenay-Luck, N., and Fernandes, D.J. (2008). The nucleolin targeting aptamer AS1411 destabilizes Bcl-2 messenger RNA in human breast cancer cells. Cancer Res. *68*, 2358–2365. https://doi.org/10.1158/0008-5472.CAN-07-5723.

36. Bompiani, K.M., Woodruff, R.S., Becker, R.,C., Nimjee, S.M., Sullenger, B.A., and Sullenger, A.B. (2012). Antidote control of aptamer therapeutics: the road to a safer class of drug agents. Curr. Pharm. Biotechnol. *13*, 1924–1934. https://doi.org/10.2174/138920112802273137.

37. Zhao, N., Pei, S.N., Qi, J., Zeng, Z., Iyer, S.P., Lin, P., Tung, C.H., and Zu, Y. (2015). Oligonucleotide aptamer-drug conjugates for targeted therapy of acute myeloid leukemia. Biomaterials *67*, 42–51. https://doi.org/10.1016/j.biomaterials.2015.07.025.

38. Kelly, L., Maier, K.E., Yan, A., and Levy, M. (2021). A comparative analysis of cell surface targeting aptamers. Nat. Commun. *12*, 6275. https://doi.org/10.1038/s41467-021-26463-w.

39. Xie, J., Mao, Q., Tai, P.W.L., He, R., Ai, J., Su, Q., Zhu, Y., Ma, H., Li, J., Gong, S., et al. (2017). Short DNA hairpins compromise recombinant adeno-associated virus genome homogeneity. Mol. Ther. *25*, 1363–1374. https://doi.org/10.1016/j.ymthe.2017.03.028.

40. Chai, S., Kim, Y., Galivo, F., Dorrell, C., Wakefield, L., Posey, J., Ackermann, A.M., Kaestner, K.H., Hebrok, M., and Grompe, M. (2022). Development of a beta cell-specific expression control element for rAAV. Hum. Gene Ther. *33*, 789–800. https://doi.org/10.1089/HUM.2021.219.

41. Mullard, A. (2021). Gene therapy community grapples with toxicity issues, as pipeline matures. Nat. Rev. Drug Discov. *20*, 804–805. https://doi.org/10.1038/D41573-021-00164-X.

42. Hordeaux, J., Buza, E.L., Dyer, C., Goode, T., Mitchell, T.W., Richman, L., Denton, N., Hinderer, C., Katz, N., Schmid, R., et al. (2020). Adeno-associated virus-induced dorsal root ganglion pathology. Hum. Gene Ther. *31*, 808–818. https://doi.org/10.1089/HUM.2020.167.

43. Chand, D., Mohr, F., McMillan, H., Tukov, F.F., Montgomery, K., Kleyn, A., Sun, R., Tauscher-Wisniewski, S., Kaufmann, P., and Kullak-Ublick, G. (2021). Hepatotoxicity following administration of onasemnogene abeparvovec (AVXS-101) for the treatment of spinal muscular atrophy. J. Hepatol. *74*, 560–566. https://doi.org/10.1016/J.JHEP.2020.11.001.

44. Johnson, J.S., Li, C., DiPrimio, N., Weinberg, M.S., McCown, T.J., and Samulski, R.J. (2010). Mutagenesis of adeno-associated virus type 2 capsid protein VP1 uncovers new roles for basic amino acids in trafficking and cell-specific transduction. J. Virol. *84*, 8888–8902. https://doi.org/10.1128/JVI.00687-10.

45. Popa-Wagner, R., Porwal, M., Kann, M., Reuss, M., Weimer, M., Florin, L., and Kleinschmidt, J.A. (2012). Impact of VP1-specific protein sequence motifs on adeno-associated virus type 2 intracellular trafficking and nuclear entry. J. Virol. *86*, 9163–9174. https://doi.org/10.1128/JVI.00282-12.

46. Bosma, B., du Plessis, F., Ehlert, E., Nijmeijer, B., de Haan, M., Petry, H., and Lubelski, J. (2018). Optimization of viral protein ratios for production of rAAV serotype 5 in the baculovirus system. Gene Ther. *25*, 415–424. https://doi.org/10.1038/s41434-018-0034-7.

47. Zhang, C., Zhou, X., Yao, T., Tian, Z., and Zhou, D. (2018). Precision fluorescent labeling of an adeno-associated virus vector to monitor the viral infection pathway. Biotechnol. J. *13*, e1700374. https://doi.org/10.1002/biot.201700374.

48. Yao, T., Zhou, X., Zhang, C., Yu, X., Tian, Z., Zhang, L., and Zhou, D. (2017). Site-specific PEGylated adeno-associated viruses with increased serum stability and reduced immunogenicity. Molecules *22*, 1155. https://doi.org/10.3390/molecules22071155.

49. Kelemen, R.E., Mukherjee, R., Cao, X., Erickson, S.B., Zheng, Y., and Chatterjee, A. (2016). A precise chemical strategy to alter the receptor specificity of the adeno-associated virus. Angew. Chem. Int. Ed. Engl. *55*, 10645–10649. https://doi.org/10.1002/anie.201604067.

50. Zhang, C., Yao, T., Zheng, Y., Li, Z., Zhang, Q., Zhang, L., and Zhou, D. (2016). Development of next generation adeno-associated viral vectors capable of selective tropism and efficient gene delivery. Biomaterials *80*, 134–145. https://doi.org/10.1016/j.biomaterials.2015.11.066.

51. Holehonnur, R., Luong, J.A., Chaturvedi, D., Ho, A., Lella, S.K., Hosek, M.P., and Ploski, J.E. (2014). Adeno-associated viral serotypes produce differing titers and differentially transduce neurons within the rat basal and lateral amygdala. BMC Neurosci. *15*, 28. https://doi.org/10.1186/1471-2202-15-28.

52. Katrekar, D., Moreno, A.M., Chen, G., Worlikar, A., and Mali, P. (2018). Oligonucleotide conjugated multi-functional adeno-associated viruses. Sci. Rep. *8*, 13589. https://doi.org/10.1038/s41598-018-21742-x.

53. Heshmati Aghda, N., Dabbaghianamiri, M., Tunnell, J.W., and Betancourt, T. (2022). Design of smart nanomedicines for effective cancer treatment. Int. J. Pharm. *621*, 121791. https://doi.org/10.1016/J.IJPHARM.2022.121791.

54. Huang, Y.W., Cambre, M., and Lee, H.J. (2017). The toxicity of nanoparticles depends on multiple molecular and physicochemical mechanisms. Int. J. Mol. Sci. *18*, 2702. https://doi.org/10.3390/IJMS18122702.

55. Buchman, J.T., Hudson-Smith, N.V., Landy, K.M., and Haynes, C.L. (2019). Understanding nanoparticle toxicity mechanisms to inform redesign strategies to reduce environmental impact. Acc. Chem. Res. *52*, 1632–1642. https://doi.org/10.1021/ACS.ACCOUNTS.9B00053.

56. Yan, A.C., and Levy, M. (2018). Aptamer-mediated delivery and cell-targeting aptamers: room for improvement. Nucleic Acid Ther. *28*, 194–199. https://doi.org/10.1089/NAT.2018.0732.

57. Stahnke, S., Lux, K., Uhrig, S., Kreppel, F., Hösel, M., Coutelle, O., Ogris, M., Hallek, M., and Büning, H. (2011). Intrinsic phospholipase A2 activity of adeno-associated virus is involved in endosomal escape of incoming particles. Virology *409*, 77–83. https://doi.org/10.1016/J.VIROL.2010.09.025.

58. Elsässer, S.J., Ernst, R.J., Walker, O.S., and Chin, J.W. (2016). Genetic code expansion in stable cell lines enables encoded chromatin modification. Nat. Methods *13*, 158–164. https://doi.org/10.1038/nmeth.3701.

59. Elsässer, S.J. (2018). Generation of stable amber suppression cell lines. In Methods in Molecular Biology (Humana Press Inc.), pp. 237–245. https://doi.org/10.1007/978-1-4939-7574-7_15.

60. Mihaila, T.S., Bäte, C., Ostersehlt, L.M., Pape, J.K., Keller-Findeisen, J., Sahl, S.J., and Hell, S.W. (2022). Enhanced incorporation of subnanometer tags into cellular proteins for fluorescence nanoscopy via optimized genetic code expansion. Proc. Natl. Acad. Sci. USA *119*. e2201861119. https://doi.org/10.1073/PNAS.2201861119.

61. Cervettini, D., Tang, S., Fried, S.D., Willis, J.C.W., Funke, L.F.H., Colwell, L.J., and Chin, J.W. (2020). Rapid discovery and evolution of orthogonal aminoacyl-tRNA synthetase–tRNA pairs. Nat. Biotechnol. *38*, 989–999. https://doi.org/10.1038/s41587-020-0479-2.

62. Zhou, J., and Rossi, J. (2017). Aptamers as targeted therapeutics: current potential and challenges. Nat. Rev. Drug Discov. *16*, 181–202. https://doi.org/10.1038/nrd.2016.199.

63. Sola, M., Menon, A.P., Moreno, B., Meraviglia-Crivelli, D., Soldevilla, M.M., Cartón-García, F., and Pastor, F. (2020). Aptamers against live targets: is in vivo SELEX finally coming to the edge? Mol. Ther. Nucleic Acids *21*, 192–204. https://doi.org/10.1016/j.omtn.2020.05.025.

64. Mi, J., Liu, Y., Rabbani, Z.N., Yang, Z., Urban, J.H., Sullenger, B.A., and Clary, B.M. (2010). In vivo selection of tumor-targeting RNA motifs. Nat. Chem. Biol. *6*, 22–24. https://doi.org/10.1038/NCHEMBIO.277.

65. Mi, J., Ray, P., Liu, J., Kuan, C.T., Xu, J., Hsu, D., Sullenger, B.A., White, R.R., and Clary, B.M. (2016). In vivo selection against human colorectal cancer xenografts identifies an aptamer that targets RNA helicase protein DHX9. Molecular therapy. Mol. Ther. Nucleic Acids *5*, e315. https://doi.org/10.1038/MTNA.2016.27.

66. Ma, C., Peng, Y., Li, H., and Chen, W. (2021). Organ-on-a-Chip: a new paradigm for drug development. Trends Pharmacol. Sci. *42*, 119–133. https://doi.org/10.1016/J.TIPS.2020.11.009.

67. Rossi, G., Manfrin, A., and Lutolf, M.P. (2018). Progress and potential in organoid research. Nat. Rev. Genet. *19*, 671–687. https://doi.org/10.1038/S41576-018-0051-9.

68. Artegiani, B., and Clevers, H. (2018). Use and application of 3D-organoid technology. Hum. Mol. Genet. *27*, R99–R107. https://doi.org/10.1093/HMG/DDY187.

69. Bashir, A., Yang, Q., Wang, J., Hoyer, S., Chou, W., McLean, C., Davis, G., Gong, Q., Armstrong, Z., Jang, J., et al. (2021). Machine learning guided aptamer refinement and discovery. Nat. Commun. *12*, 2366. https://doi.org/10.1038/s41467-021-22555-9.

70. Tunyasuvunakool, K., Adler, J., Wu, Z., Green, T., Zielinski, M., Žídek, A., Bridgland, A., Cowie, A., Meyer, C., Laydon, A., et al. (2021). Highly accurate protein structure

prediction for the human proteome. Nature *596*, 590–596. https://doi.org/10.1038/s41586-021-03828-1.

71. Jumper, J., Evans, R., Pritzel, A., Green, T., Figurnov, M., Ronneberger, O., Tunyasuvunakool, K., Bates, R., Žídek, A., Potapenko, A., et al. (2021). Highly accurate protein structure prediction with AlphaFold. Nature *596*, 583–589. https://doi.org/10.1038/S41586-021-03819-2.

72. Grimm, D., Pandey, K., Nakai, H., Storm, T.A., and Kay, M.A. (2006). Liver transduction with recombinant adeno-associated virus is primarily restricted by capsid serotype not vector genotype. J. Virol. *80*, 426–439. https://doi.org/10.1128/JVI.80.1.426-439.2006.

73. Zhang, Z., Tang, C., Hammink, R., Nelissen, F.H.T., Heus, H.A., and Kouwer, P.H.J. (2021). Multivalent Sgc8c-aptamer decorated polymer scaffolds for leukemia targeting. Chem. Commun. *57*, 2744–2747. https://doi.org/10.1039/d0cc08205h.

74. Wilner, S.E., Wengerter, B., Maier, K., de Lourdes Borba Magalhães, M., Del Amo, D.S., Pai, S., Opazo, F., Rizzoli, S.O., Yan, A., and Levy, M. (2012). An RNA alternative to human transferrin: a new tool for targeting human cells. Mol. Ther. Nucleic Acids *1*, e21. https://doi.org/10.1038/mtna.2012.14.